Hindawi
Advances in Civil Engineering
Volume 2020, Article ID 9709417, 13 pages
https://doi.org/10.1155/2020/9709417

Research Article

Research and Application of a Smart Monitoring System to Monitor the Deformation of a Dam and a Slope

Yongfei Wang,[1,2,3] Dingbin Shen,[3] Jiankang Chen,[1,2] Liang Pei,[1,2] Yanling Li,[1,2] Xiang Lu,[1,2] and Lei Zhang[4]

[1]*State Key Laboratory of Hydraulics and Mountain River Engineering, Sichuan University, Chengdu 610065, Sichuan, China*
[2]*College of Water Resources & Hydropower, Sichuan University, Chengdu 610065, Sichuan, China*
[3]*Dam Management Center of Dadu River Hydropower Development Co., Ltd., Chengdu 610065, Sichuan, China*
[4]*Chengdu Geo Space-Time Science & Technology Co., Ltd., Chengdu 610065, Sichuan, China*

Correspondence should be addressed to Liang Pei; pl_scu@scu.edu.cn

Received 10 January 2020; Revised 14 August 2020; Accepted 29 October 2020; Published 12 November 2020

Academic Editor: Zaobao Liu

Deformation monitoring is one of the most important means of providing feedback to ensure the safety of projects. Problems plague the existing automatic monitoring system, such as the small monitoring range of monitoring devices, the inadequate field safety protection, and the low accuracy under extreme weather conditions. These problems greatly reduce the real time and reliability of deformation monitoring data and restrict the real-time intelligent control of engineering safety risk. In this paper, a multitype instrument-integrated monitoring system based mainly on the total positioning station (TPS) and supplemented by the Global Navigation Satellite System (GNSS) was promoted with the methods of large field angle, data complementation, environmental perception and judgment, automatic status control, and baseline calibration-meteorological fusion correction. The application results of Pubugou Station show that the averages of mean square error of points (APMSE) for the dam are 0.41~1.65 mm and the averages of mean square error of height (AHMSE) are 0.42~0.89 mm. Moreover, the APMSE and AHMSE for the slope are less than 3 mm. The maximum relative error of the TPS and GNSS data compared with the artificial monitoring data is less than 10%. Besides, the system has good overall performance and is of significant comprehensive benefits. The proposed system realizes the all-weather real-time monitoring of deformation and enhances the emergency response capability of special conditions in dams during the operation period.

1. Introduction

Hydropower projects are the indispensable basis of national economic and social development because such projects involve the smart management, control, and linkage response of safety risk, which is a strategic demand for the national information industry and smart energy development. Deformation monitoring is an important support for the scientific assessment of real-time safety risk of dams and reservoir slopes. However, the traditional monitoring of deformation has such problems as low efficiency, high operational risk, slow feedback, and low regularity of data. These problems greatly reduce the real time and reliability of deformation monitoring data and restrict the real-time intelligent control of engineering safety risk. Developing a method to acquire high-confidence real-time data intelligently under complex environments (e.g., unfavourable weather, high-risk slopes, and field risks) has been a problem that has plagued the industry.

To date, great progress in monitoring automation has been made, and many practical software systems and monitoring technologies have been developed at home and abroad [1–7], such as the three-dimensional (3D) laser scanning technology [8–10], remote sensing technology [11, 12], surveying robot technology [13], and optical time domain reflection technology [14]. The Geomatic Monitoring System (GeoMos) of Leica in Switzerland, the Deformation Monitoring System (DIMONS) of New Brunswick University in Canada, and the automatic deformation monitoring system (AutoMos) are representative deformation automation monitoring systems [15–17]. Moreover, some interesting results have been reported. Yang et al. [18]

studied an automatic monitoring system including monitoring modules, data acquisition module, and data processing module to overcome the plateau climate and frozen soil. Zhang et al. [19] developed the deformation monitoring system Georobot Deformation Monitoring System (GRT-DEMOS), which has been tested successfully in the east landslide section of the Three Gorges Project Reservoir Area. The research above shows that there are the following selected problems in the existing automatic deformation monitoring stations and systems: (1) enough stations are needed for the large-scale hydropower projects because the field angle of a station and the monitoring range of a single surveying robot are small, leading to a higher invested cost and postmaintenance workload; (2) qualified or high-accuracy monitoring data cannot be obtained under extreme weather conditions, such as torrential rain and strong wind due to the difficulties in identifying the external environment and select a suitable measurement time intelligently; (3) the measurement accuracy and long-term stability of equipment operation performance are hard to guarantee due to the influence of temperature and humidity inside the stations. What is worse, the damage risk of stations without comprehensive protection measures in the field is very high because of the unfavourable weather conditions. With more and more attention paid to the safety of water conservancy projects, the online real-time control and early warning of physical quantities that affect or characterize engineering safety are necessary, such as the flood, the deformation, and the rainfall [20–25]. Aiming at the problems existing in the current deformation online monitoring system, the objective of this paper is to develop a high-accuracy remote smart monitoring system for deformation to improve the real-time, intelligent, and reliable property of deformation monitoring enabling the aspects of a smart station of the protection of exact instruments, remote control, data acquisition, and early warning.

A multitype instrument-integrated monitoring system based mainly on the total positioning station (TPS) and supplemented by the Global Navigation Satellite System (GNSS) is promoted in the paper, and a smart station platform of deformation integrating large field angle, environmental real-time identification, self-selection of the measurement period, automatic adjustment of station status, and baseline calibration-meteorological fusion correction is constructed. It realizes the real-time smart acquisition of high-confidence monitoring data in a complex environment and enhances the emergency response capability of special conditions in dams during the operation period.

2. Integrative Smart Station Platform of Deformation Monitoring

2.1. Overall Framework and Measurement Process

2.1.1. Overall Framework. The main modules of the smart station platform based on the large field angle method to increase the monitoring range are the deformation monitoring station host (DMSH), the TPS, and the GNSS, as shown in Figure 1.

The DMSH module can realize the intelligent perception of environmental conditions, the automatic control of the storage environment of the exact instruments, the real-time monitoring of the operation conditions, the automatic regulation of temperature and humidity, the acquisition of basic meteorological parameters, the intelligent selection of the time to open or close the observation window of a station automatically (periodically or in real time), and the cooperation with the measuring robot to complete the deformation monitoring task.

The functions of the TPS module mainly involve the grouping of monitoring information, task formulation, data quality control, and backup. The TPS is the main means of measuring station platform. Besides, the baseline calibration-meteorological fusion correction method is proposed considering the uncertainty of the atmospheric vertical refraction coefficient on the basis of quality control in the traditional meteorological correction method; the baseline calibration-meteorological fusion correction coefficient and the atmospheric refraction coefficient from the smart station to monitoring points can be calculated using the interpolated algorithm. By these means, the unilateral monitoring accuracy of triangulated height will be improved by updating the original monitoring data from the TPS (the horizontal angle, vertical angle, and slant distance).

The sampling adjustment, data detection, and exceptional cases are expressed in the GNSS module, which can assist the measurement of TPS and complete the monitoring task at a regular time. The coaxial installation of multitype precise observation equipment and the mutual complementation of different monitoring data sources are achieved by the concurrent monitoring of TPS-GNSS.

2.1.2. Measurement Process. According to the framework of the integrated smart station platform, the intelligent monitoring measurement process of deformation mainly includes Part A and Part B, as shown in Figure 2.

(i) *Part A. The Intelligent Data Acquisition of TPS*

Section a. After starting the monitoring task through the smart station platform constructed by the large field angle method, the wind speed and rainfall conditions are judged first. If the external environment conditions do not meet the setting requirements (which can be set according to the user needs), then the monitoring task will be abandoned, or the safety cover will be open to allow the surveying robot to adapt to the external temperature within one hour. Afterward, the condition of wind speed and rainfall will be in the real-time monitoring state for a while. Note that the monitoring task will be cancelled if the environmental conditions cannot satisfy the demands during a measurement process.

Section b. The observation options and related parameters, such as the measuring accuracy of the angle, the measuring accuracy of the side, the tolerance, and the projection direction, are preset during the monitoring of TPS. After the data are collected, the baseline calibration-meteorological fusion correction coefficient is determined by the known information between the

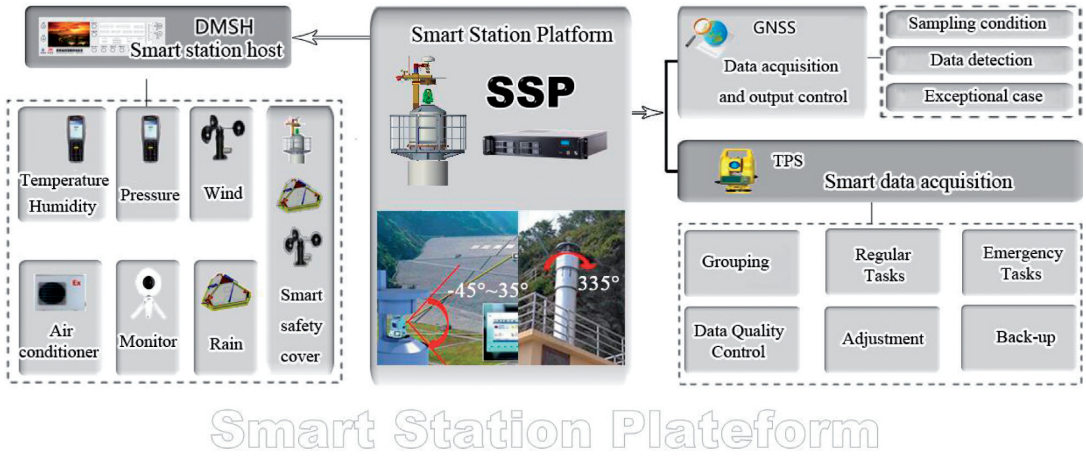

Figure 1: Framework of the integrated smart station platform.

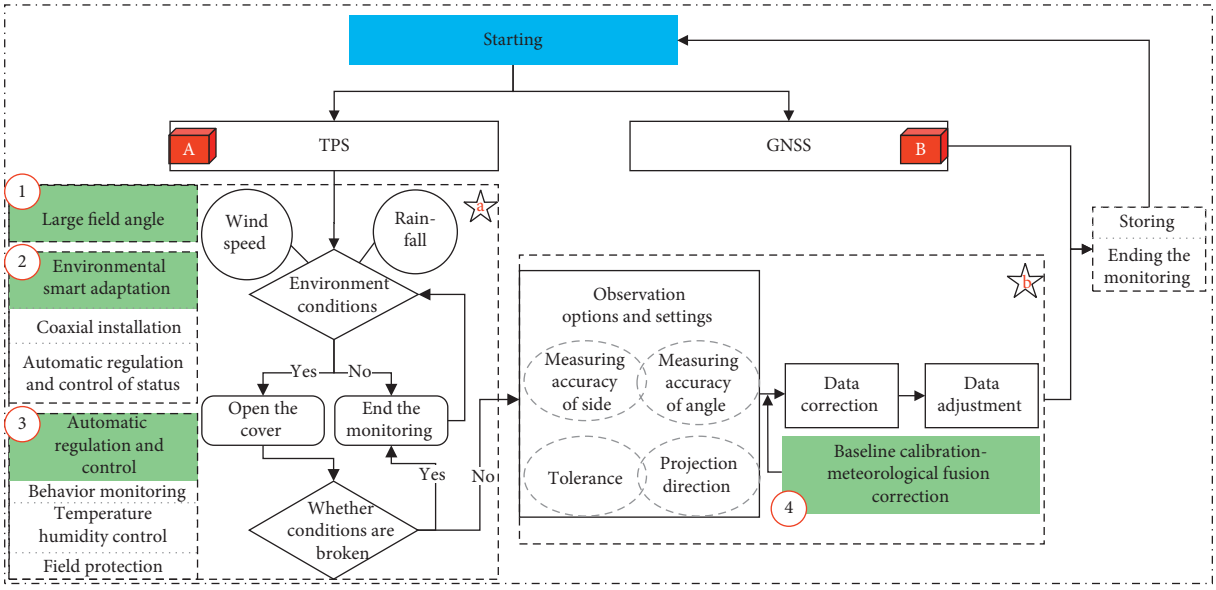

Figure 2: Smart measurement process of deformation.

smart station and the control points based on the baseline calibration-meteorological fusion correction method; subsequently, the horizontal angle, vertical angle, and slant distance of the original observation data can be corrected. Finally, the adjusted data are stored in the database.

(ii) *Part B. The Data Acquisition of GNSS.*

The data acquisition of GNSS is measured regularly every 24 hours (settable), and the measurement results are stored directly.

2.2. Methods. All four key technologies of the large field angle, environmental smart adaptation, automatic regulation and control of the station status, and baseline calibration-meteorological fusion correction are introduced in the smart station platform.

2.2.1. Large Field Angle. In general, the horizontal field angle of the surveying robot placed in the observation room can reach up to 150° at most through a viewing window, and sometimes can be up to 200° through a curved window; such a robot is unable to adapt to the needs of large hydropower projects of monitoring the dam crest, dam slope, network point, and slopes. By heightening the observation pier and adopting a 360° cylindrical lifting window, the horizontal and vertical field angles of the promoted smart station platform can be approximately 335° and − 45°~35°, respectively. This technology greatly increases the monitoring range of the single station, reducing the cost of building multiple stations and realizes the monitoring task of large-scale regions with a minimum number of stations in actual engineering projects, as shown in Figure 3.

Figure 3: Drawing of the large field angle in the smart station.

2.2.2. Environmental Smart Adaptation

(1) *Complementation of Monitoring Data*

The TPS monitoring prism and the GNSS aerial are installed (TPS-GNSS) coaxially to realize the mutual complementation of different monitoring data sources (shown in Figure 4(a)), leading to a comprehensive analysis of the deformation and providing more accurate and reliable deformation monitoring results. The design of complementation not only can effectively solve the problem that TPS has difficulty in collecting effective data quickly and providing feedbacks timely but also can strengthen the observation of points with a long measuring line or in the reservoir area.

(2) *Environmental Perception and Judgment*

Based on the automatic monitoring at a fixed time, the traditional automatic monitoring system of deformation cannot acquire qualified data under adverse weather, such as rain, snow, fog, and strong sunlight. The designed smart station platform with the functions of environmental perception and judgment can select the time to open the safety cover and the time of observation to avoid the risk of opening the safety cover and performing measurements under the conditions of heavy wind and rain, thereby improving the overall quality of the deformation monitoring data. The rain sensor is shown in Figure 4(b).

Besides, the temperature sensors are set up to measure the change of the temperature gradient. The conditions of no wind (less than 4 m/s), no rain (less than 5 mm/12 h), high visibility (more than 700 m), and stable temperature and pressure are selected intelligently to minimize the effect of weather conditions on the observation precision.

2.2.3. Automatic Regulation and Control of the Station Status. The temperature and humidity of the station change periodically with the season because the intelligent surveying robots, prisms, GNSS aerial, and other precision instruments are located in the field, and the annual temperature variation will exceed 50°C sometimes; such variations are not conducive to the long-term stable operation of precision instruments and have great influences on the instrument operating status, accuracy, and reliability of data. Therefore, the video monitoring system, the temperature, and the humidity monitoring system and the smart automatic opening and closing system of air conditioning are installed to adapt to the changing environment. The annual temperature variation of the integrated station is approximately 20°C in one year through the automatic temperature adjustment of the air conditioner. Moreover, the real-time temperature and humidity conditions can be used as the basic parameters of meteorological correction. The protection and working statuses of the station in the field are often shown via video monitoring.

2.2.4. Baseline Calibration-Meteorological Fusion Correction. The influences of the meteorological conditions, earth curvature, and refraction and the long-term stability of instruments on the distance measurement cannot be ignored in the automatic deformation monitoring system. However, the uncertainty of the atmospheric vertical refraction coefficient and the representative error of the surveying robot are not considered in the traditional meteorological correction method, which has some influence on the accuracy of the deformation sequences. To address this issue, a baseline calibration-meteorological fusion correction is introduced in the integrated station platform by using the known information between the stations and the control points.

The difference between the actual observation data and the coordinate inverse calculation data is calculated by the actual observation data (horizontal angle, vertical angle, and slant range) between the station and the control point. First, the known slant distance $d^0_{S_0X_i}$ and the measured slant distance $d^i_{S_0X_i}$ between station S_0 and control point X_i is performed in the following equations:

$$d^0_{S_0X_i} = \sqrt{(x_0 - x_i)^2 + (y_0 - y_i)^2 + (H_0 - H_i)^2}, \quad (1)$$

$$d^i_{S_0X_i} = \sqrt{(x_0 - x_i')^2 + (y_0 - y_i')^2 + (H_0 - H_i')^2}, \quad (2)$$

where (x_i, y_i, H_i) is the coordinate information of the control point X_i; (x_0, y_0, H_0) is the coordinate information of station S_0; (x_i', y_i', H_i') is the actual measurement coordinate information of control point X_i; and i is the number of control points $(i \geq 3)$.

The slant distance of the TM30 surveying robot resulting from the meteorological conditions is shown in the following equation:

$$\Delta S = \Delta S_1 + \Delta S_2 = \left(\mathrm{ak} + \mathrm{bk} \cdot S \times 10^{-3}\right) + \left(0.29 - \frac{0.30 \times 10^{-3} \cdot p}{(1 + \alpha t)} - \frac{4.13 \times 10^{-7} \cdot h}{(1 + \alpha t)} \cdot 10^{x}\right) \cdot S, \quad (3)$$

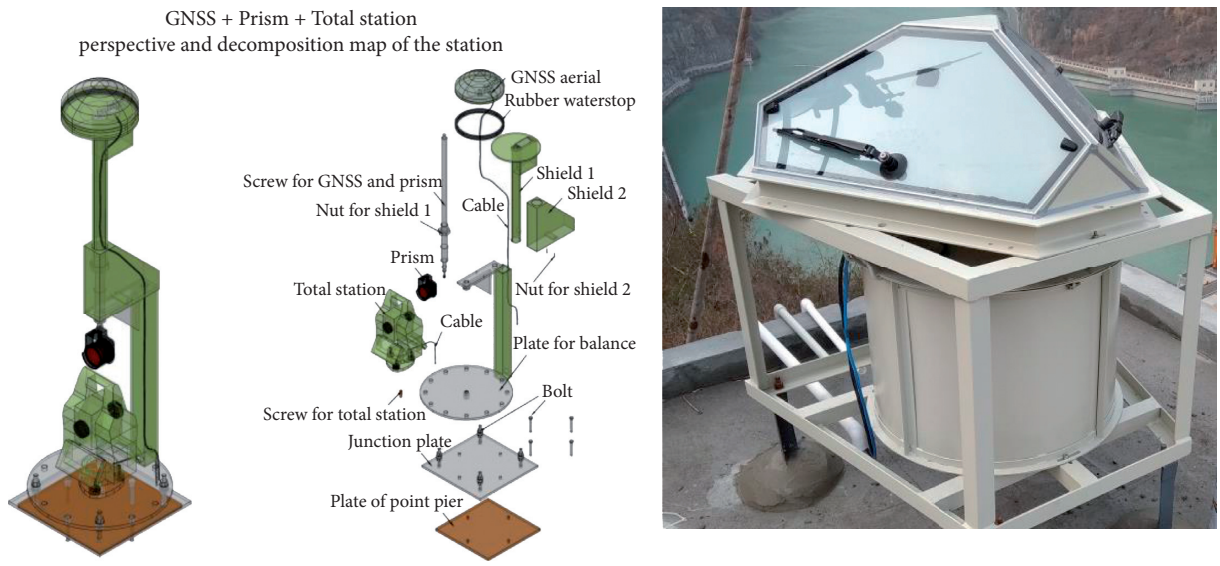

Figure 4: Diagram of the (a) TPS-GNSS and (b) the rain sensor.

where ΔS is the correction value of distance, mm; ΔS_1 is the correction value of the additive constant and multiplicative constant, mm; ΔS_2 is the meteorological correction value, mm; ak is the additive constant, mm; bk is the multiplicative constant, ppm; S is the measured distance, m; p, h, and t are the pressure (hPa), dry temperature (°C), and relative humidity (%), respectively, and the values of them are 1013.25 hPa, 12°C, and 60%, respectively, based on the meteorological value in the dam; α is the atmospheric expansion coefficient, with $\alpha = (1/273.15)$; and x is the humidity index, with $x = (7.5t/(237.3 + t) + 0.79)$.

According to equations (1)–(3), the baseline calibration-meteorological fusion correction coefficient p_i can be given, as shown in the following equation:

$$p_i = \frac{d^i_{S_0X_i} - d^0_{S_0X_i} - \Delta S}{d^i_{S_0X_i}}. \tag{4}$$

In addition, the influence of atmospheric refraction and Earth curvature should be also considered on the basis of baseline calibration-meteorological fusion correction, and the atmospheric refraction coefficient k_i can be expressed based on the principle of geometric triangulation [26]:

$$k_i = 1 + \frac{2R}{D^2}(D\tan\alpha + i - v - h_{0i}), \tag{5}$$

$$h_{0i} = D\tan\alpha + \frac{1 - k_i}{2R}D^2 + i - v, \tag{6}$$

where h_{0i} is the elevation difference between points of S_0 and X_i; D is the horizontal distance between points of S_0 and X_i; α is the vertical angle; R is the radius of Earth curvature with the value of 6371 km; i is the height of instrument height in point of S_0; and v is the height of the prism in X_i.

In practical engineering projects, the deformation monitoring areas of the dam and slope have the characteristics of large altitude differences, wide scope, and lots of measuring points; thus, the limited control points at different elevations play an important role in the distance correction. The monitoring points in a dam or slope are usually arranged with the same elevation as a unit, and several elevation units are designed. It is noted that the meteorological condition at the same elevation in the dam or slope areas is almost the same. Therefore, to determine the baseline calibration-meteorological fusion correction coefficient p_i and the atmospheric refraction coefficient k_i of each measuring point, an interpolated model combining the equal elevation-based hierarchical observation scheme is proposed to greatly reduce the internal meteorological gradient change of each elevation. The commonly used interpolation methods in data processing are the nearest neighbor interpolation, bilinear interpolated, B-spline interpolation, convolution interpolation, Lagrange interpolation, Newton interpolation, Hermite interpolation, and polynomial piecewise interpolation algorithms [27, 28], in which the bilinear interpolated model is an interpolation method for two variables and is suitable to be adopted for the correction analysis of deformation monitoring in the measuring points at the same elevation. The model is shown in the following equation:

$$f(x, y) = a_0 + a_1x + a_2y + a_3xy, \tag{7}$$

where $f(x, y)$ is the trend surface for baseline calibration-meteorological fusion correction coefficient and the atmospheric refraction coefficient; x, y is the coordinate information of a point; and a_0, a_1, a_2, and a_3 are the coefficients to be solved and can be solved by the least square method.

Based on equations (1)–(7), the 3D coordinate information of the measuring points is obtained with the corrected monitoring data and the coordinate information of S_0.

3. Case Study

3.1. Project Background

3.1.1. Dam Specifications. The Pubugou Hydropower Station is located on the Dadu River on the border between Hanyuan County and Ganluo County, Sichuan Province, China. This enormous hydroelectric project has a total electric generating capacity of 3600 MW and the ability to seasonally regulate output. The storage capacity is 5.39 billion m^3, the maximum height of the dam is 186 m, and the normal water storage level is 850.00 m. The hydropower station is mainly composed of three parts: a core rockfill dam, a water power generation system, and a discharge structure, as seen in Figure 5.

3.1.2. Monitoring Layout Design. An integrated intelligent station scheme is adopted for the deformation monitoring of the dam and the slope in Pubugou Hydropower Station, including the "TB02" station (back of dam) and the "TB01" station (front of the dam), the measuring points (Measuring PT), network points (Network PT), and the back sight points (BKS PT), as shown in Figure 6. The deformation monitoring points of the dam are arranged in the dam crest (EL.856.00 m), the benches (EL.806.00 m and EL.756.00 m), and the downstream pressure zones (EL.731.00 m (U) and EL.731.00 m (D)). Moreover, three groups of points are designed in the horse road (1-1 section) and the upper part (2-2 and 3-3 sections) of the tension-displaced body in front of the dam. The number and location of points are shown in Figure 7. Besides, GNSS prisms are placed on the points of TP13, TP21, TP27, and TP32 to form concurrent monitoring with the TPS. The deformation smart station platform of Pubugou Hydropower Station was completed and began operation in 2015; the smart station platform realized the all-weather real-time monitoring of the dam and the slope and increased the emergency disposal ability under special conditions such as heavy rainfall and earthquake.

3.2. Results and Analysis

3.2.1. Reliability Evaluation of Monitoring Data. The average mean square error of height (AHMSE) and the average mean square error of point (APMSE) are selected as the accuracy evaluation indicators of the monitoring data concerning the GB 50026-2007 [29]. The average mean square error (AMSE), including the AHMSE and APMSE, is the average of multiple mean square errors (MSE) of the measuring points in a day. The mean square error of height (HMSE) and mean square error of point (PMSE) of a point on the i^{th} day are expressed by the following equations:

$$\mathrm{HMSE}_i = \sqrt{\frac{1}{n}\sum_{k=1}^{n}\left(Z_k^i - \overline{Z}^i\right)^2}, \tag{8}$$

$$\mathrm{PMSE}_i = \sqrt{\mathrm{XMSE}_i^2 + \mathrm{YMSE}_i^2}, \tag{9}$$

$$\mathrm{XMSE}_i = \sqrt{\frac{1}{n}\sum_{k=1}^{n}\left(X_k^i - \overline{X}^i\right)^2}, \tag{10}$$

$$\mathrm{YMSE}_i = \sqrt{\frac{1}{n}\sum_{k=1}^{n}\left(Y_k^i - \overline{Y}^i\right)^2}, \tag{11}$$

where HMSE_i, PMSE_i, XMSE_i, and YMSE_i are the mean square error of height, the mean square error of point, the mean square error of horizontal displacement across the river, and the mean square error of horizontal displacement along the river on the i^{th} day, respectively; X_k^i, Y_k^i, and Z_k^i are the horizontal displacement across the river, the horizontal displacement along the river, and the elevation of the k^{th} observation on the i^{th} day, respectively; $\overline{X}$, $\overline{Y}$, and $\overline{Z}$ are the corresponding mean values of n observations; and n is the number of observations on the i^{th} day.

Therefore, the calculation formulas of AHMSE and APMSE are shown in the following equations:

$$\mathrm{AHMSE} = \frac{\sum_{i=1}^{m}\mathrm{HMSE}_i}{m}, \tag{12}$$

$$\mathrm{APMSE} = \frac{\sum_{i=1}^{m}\mathrm{PMSE}_i}{m}, \tag{13}$$

where m is the time range of measurement accuracy evaluation (day).

(1) Dam. Figures 8 and 9 show the MSE accuracy of monitoring points of the dam from July 2014 to May 2018. As shown in Figure 8, the APMSE of points in the Pubugou dam is small and is controlled between 0.41 mm and 1.65 mm, which is in line with the accuracy requirements of the second deformation monitoring (3 mm). Also, the AHMSE is controlled between 0.19 mm and 0.89 mm. The points at EL.856.00 m and EL.806.00 m do not meet the accuracy requirements of the second deformation monitoring (0.5 mm) but can meet the accuracy requirements of the third deformation monitoring (1.0 mm).

Although the AHMSE of some points cannot meet the accuracy requirements of the second deformation monitoring (ARSDM), it does not mean that all MSEs of those points do not satisfy the ARSDM. Figure 9 shows the ratio (RM) of measuring the accuracy of different measuring points during the monitoring period lower than the ARSDM. The RM of HMSE is found to be significantly different at different elevations. The maximum RM is up to 55.31% in the point of TP 10Z at the elevation of 856.00 m (Dam crest), in which the fluctuation range of RM is 34.37%~55.31%. The minimum RM is as low as 2.02% in the point of TP 38 at the elevation of 731.00 m (D), in which the fluctuation range of RM is 2.02%~7.52%. For the points at the elevation of 756.00 m, the fluctuation range of RM is 7.86%~34.04%. It can be found that the RM at a high elevation is higher than that at a low elevation, and the reason may be that the accuracy of the deformation of points at

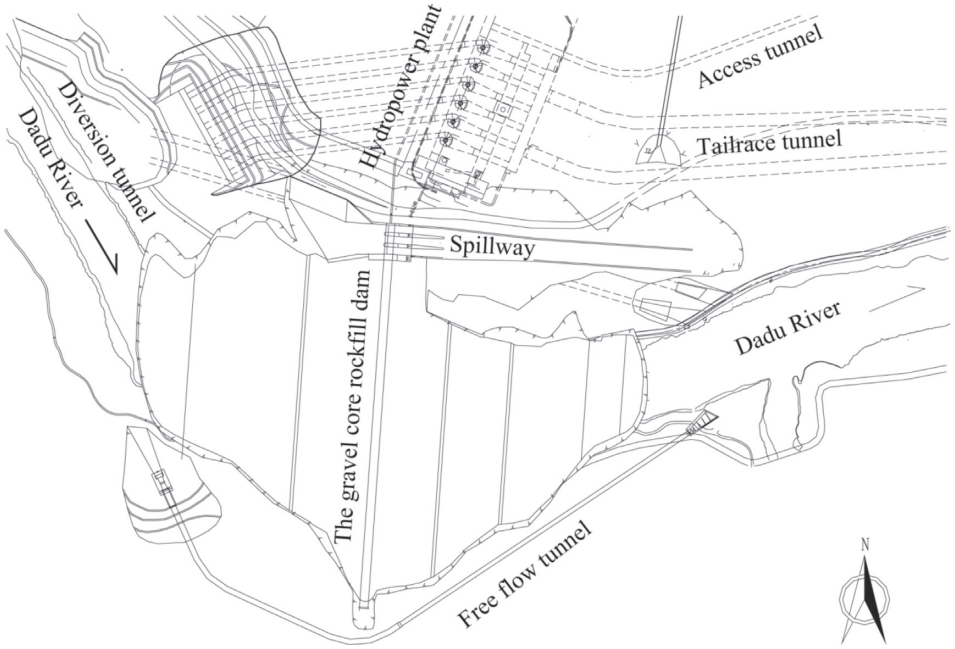

Figure 5: The layout of the Pubugou hydropower station.

Figure 6: Layout of the deformation measuring points in the Pubugou hydropower station.

different elevations is affected by the location and elevation of the smart station. Therefore, the relationship between location and accuracy is the key issue to be solved in future research. Moreover, the RM of PMSE is very small, with measuring accuracy of almost all points being in line with the requirements.

(2) Slope. The AMSE results of the slope monitoring system are shown in Table 1. It can be seen that the maximum APMSE of slope measuring points is 2.84 mm, whereas the minimum is 0.94 mm; the maximum and minimum values of AHMSE are 1.85 mm and 1.48 mm, respectively, which satisfy the allowable AMSE with the value of ±3 mm in

(a) (b)

Figure 7: Measuring points of (a) the dam and (b) the slope.

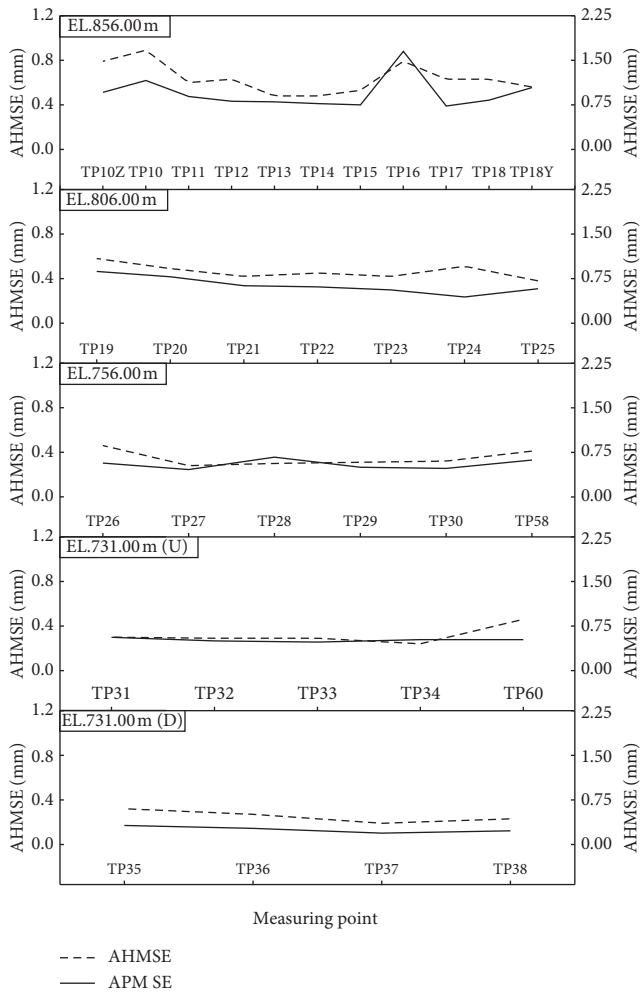

Figure 8: AHMSE and APMSE of the monitoring data.

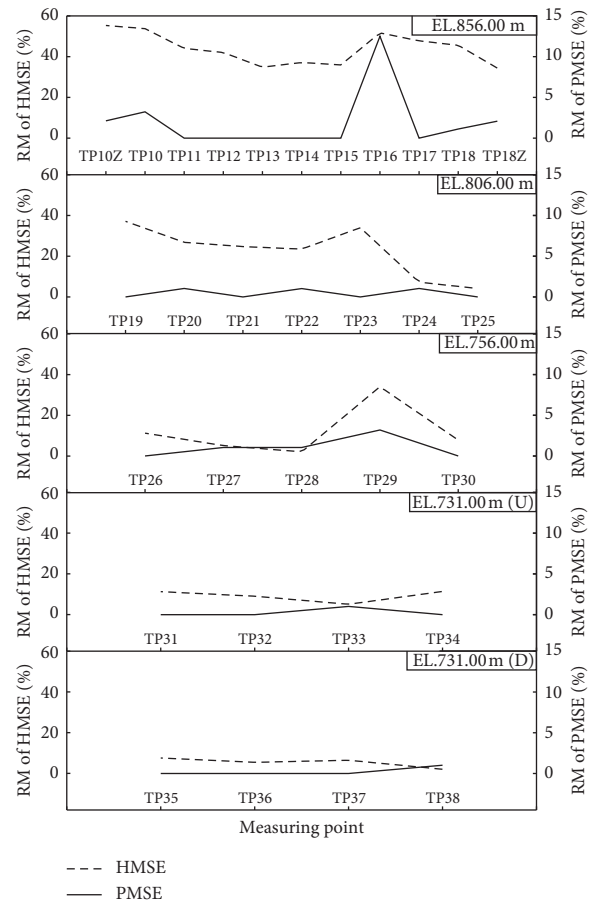

Figure 9: RM of HMSE and PMSE.

SL197-2013 [30], indicating that the proposed deformation monitoring system meets the accuracy requirements of slope monitoring.

3.2.2. Concurrent Monitoring Analysis of TPS-GNSS. The comparative analysis results of TPS-GNSS concurrent monitoring show that the fluctuation range of data from TPS is larger than that of data from GNSS in a certain time, and the latter has better continuity than that of the former, as shown in Figure 10.

Table 1: Statistical results of AMSE in the slope monitoring system.

Section	Number	APMSE (mm)	AHMSE (mm)
1-1	T05	1.44	1.14
	T06	1.61	1.25
	T07	1.21	0.61
	T08	1.29	0.85
	T22	0.97	0.63
	T21	1.08	0.73
2-2	T01	1.25	1.85
	T02	1.33	0.73
	T03	1.51	1.05
	T04	0.94	0.74
	T16	1.51	1.09
	T20	1.29	0.48
3-3	T13	2.31	0.95
	T14	2.84	1.02
	T15	1.46	0.81
	T17	1.98	1.05
	T18	1.92	1.04
	T19	2.10	0.96

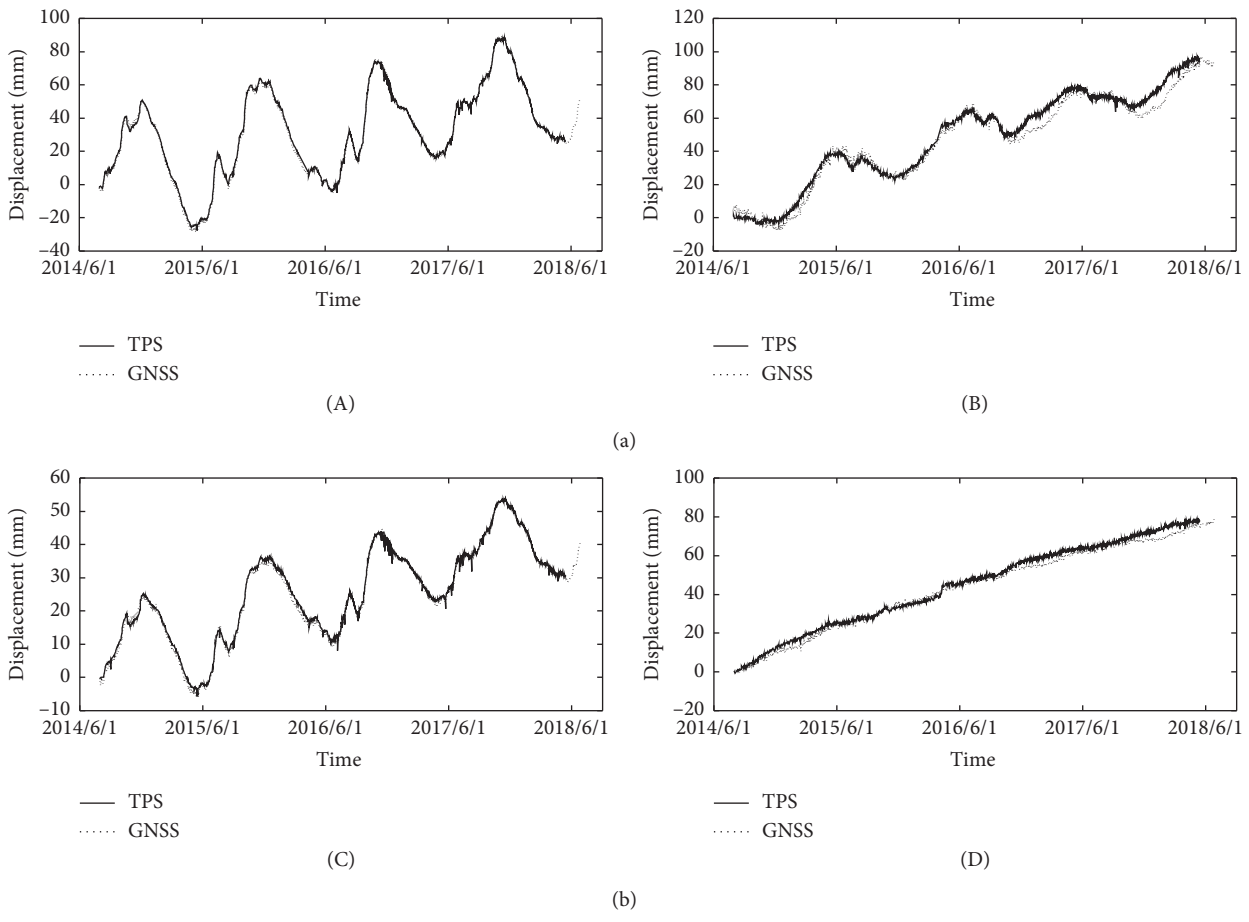

Figure 10: Continued.

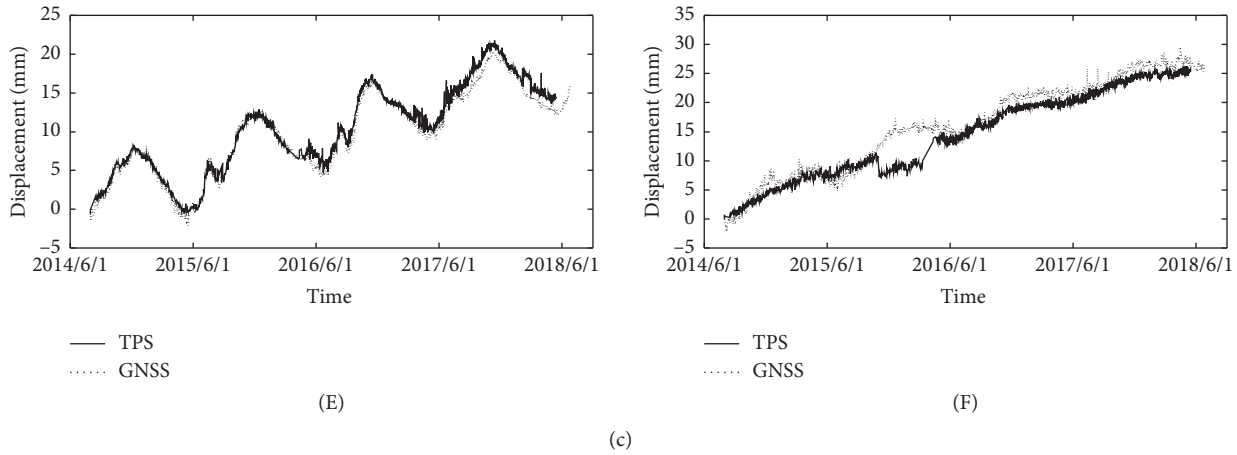

Figure 10: Comparison of displacements obtained from the TPS-GNSS monitoring. (a) TP13: (A) horizontal, (B) vertical; (b) TP21: (C) horizontal, (D) vertical; (c) TP27: (E) horizontal, (F) vertical.

Undeniably, there are some abnormal monitoring data due to the environmental influence that cannot be offset by the baseline calibration-meteorological fusion correction method. Based on the data from GNSS, the error fluctuation of deformation along the stream direction is approximately 12%, and that of vertical displacement is approximately 20%. The high error phenomenon of vertical displacement is consistent with the above conclusion that the monitoring system is not sufficiently accurate at a higher elevation. In general, the monitoring results from two monitoring methods display the same trend of deformation and have high consistency, indicating that the deformation condition reflected by the monitoring results is reliable.

3.2.3. Comparative Analysis with the Artificial Monitoring Data. The "Comprehensive Analysis on Dam Operation Performance of Pubugou Hydropower Station" [31] shows that the accuracy of the artificial monitoring data during the first six-year operation period is within the range required by the standards [29, 30]. Therefore, a comparative analysis between the artificial monitoring data and the TPS-GNSS monitoring data is made to further verify the monitoring accuracy of external deformation intelligent station based on TPS-GNSS.

In view that only the artificial monitoring of vertical deformation remains, the comparative analysis results of vertical deformation between the years of 2015 and 2018 are shown in Table 2. As seen in Table 2, the maximum relative error of the TPS data is 9.98% compared with the artificial monitoring data being 9.98%, and the maximum relative error of more than 50% points is less than 5%. The average relative error of 63% points is less than 2%. Table 3 shows the relative error of TPS-GNSS concurrent monitoring data compared with the artificial monitoring data. It can be found

Table 2: Relative error between the TPS data and artificial monitoring data.

Elevation	Points	Relative error to artificial monitoring (%)		
		Max.	Min.	Aver.
EL.856.00	TP10Z	7.90	0.00	0.35
	TP10	3.17	0.01	1.07
	TP11	1.58	0.01	0.57
	TP12	0.98a	0.01	0.31
	TP13	1.20	0.00	0.33
	TP14	0.95	0.01	0.30
	TP15	1.19	0.01	0.30
	TP16	1.34	0.01	0.52
	TP17	1.96	0.01	0.74
	TP18	8.63	0.01	2.89
	TP18Y	8.53	0.00	0.43
EL.806.00	TP19	5.58	0.07	2.71
	TP20	2.64	0.09	1.25
	TP21	1.12	0.02	0.39
	TP22	1.24	0.00	0.35
	TP23	2.91	0.01	1.04
	TP24	1.34	0.00	0.35
	TP25	6.00	0.04	1.97
EL.756.00	TP26	8.38	0.04	3.03
	TP27	2.13	0.12	1.31
	TP28	3.45	0.03	1.22
	TP29	5.03	0.03	1.45
	TP30	9.98	0.14	3.57
EL.731.00 (U)	TP31	8.96	1.02	5.35
	TP32	5.65	0.25	2.77
	TP33	9.41	0.06	4.31
	TP34	9.49	0.14	4.63
EL.731.00 (D)	TP35	5.30	0.02	2.78
	TP36	7.65	0.16	4.01
	TP37	6.36	0.00	2.88
	TP38	8.78	0.25	4.23

Table 3: Relative error between the TPS-GNSS concurrent monitoring data and artificial monitoring data.

Points and modes		Relative error to artificial monitoring (%)		
		Max.	Min.	Aver.
TP13	TPS	0.99	0.00	0.27
	GNSS	1.86	0.03	0.97
TP21	TPS	0.67	0.02	0.34
	GNSS	1.04	0.02	0.36
TP27	TPS	2.13	0.17	1.05
	GNSS	2.85	0.04	1.18

that the results of artificial monitoring, TPS monitoring, and GNSS monitoring are consistent, and their deformation trend and change law are the same. The relative error of TPS data is lower than those of GNSS data compared with the artificial monitoring data. The results illustrate that the TPS and TPS-GNSS monitoring results are consistent with artificial monitoring results, displaying that the system is of high accuracy and can meet the engineering requirements of the external deformation monitoring of Pubugou hydropower station.

3.2.4. Evaluation of the System Performance and Comprehensive Benefit

(1) System Performance. The system performance can be assessed by the mean time between failures (MTBF) within the assessment period of one year, the definition of which is [32]

$$\text{MTBF} = \frac{\sum_{i=1}^{n} t_i}{\left(\sum_{i=1}^{n} r_i\right)}, \tag{14}$$

where t_i is the normal working times of the i^{th} acquisition unit; r_i is the number of failures of the i^{th} acquisition unit; and n is the total number of data acquisition unit.

Table 4 shows the MTBF of the seven data acquisition units in the system. The MTBF of the system is 7644 h, and it is greater than the allowable threshold of 6300 h [32]. Results imply that the overall operating performance of the system is good, which meets the needs of practical engineering and plays an important role in the safe operation of the Pubugogou high core rockfill dam.

(2) Comprehensive Benefit. The comprehensive benefit of this system is studied from aspects of the economic and efficiency fronts.

On the economic front, the designed five TM30 surveying robots with the unit price of 250,000 Renminbi (RMB) are replaced by two smart stations with the unit price of 500,000 RMB, thereby leading to the direct saving of equipment cost of 250,000 RMB. Additionally, the number of survey person is reduced from 6 to 1, with the saving of labor cost of 600,000 RMB.

On the efficiency front, the time for finishing the monitoring tasks and interpreting data of the smart system is about 10 mins, while that of the traditional surveying robot is about 1 week. The application of smart stations greatly improves the effectiveness of deformation monitoring in the Pubugou dam, provides the technical support for intensive monitoring, and reduces the safety risk of survey persons during the trip to and from the stations under the mountain occurrence environment. Results illustrate that this smart system is of significant comprehensive benefits.

Table 4: The mean time between failures of the acquisition units in the Pubugou dam.

Data acquisition unit	Normal working times (h)	Number of failures
TPS in TB01	8736	3
TPS in TB02	8712	2
GNSS in TB01	8760	0
GNSS in TB02	8736	1
GNSS in TP13	8760	0
GNSS in TP21	8712	1
GNSS in TP27	8736	1
Sum	61152	8
MTBF of this system	7644	

4. Conclusions

(1) In view of the general problems such as small monitoring range, inadequate field safety protection, and low monitoring accuracy under extreme weather conditions in the traditional monitoring system for deformation in dams, which greatly restricts the real-time intelligent control of engineering safety risk, a multitype instrument-integrated monitoring system based mainly on the TPS and supplemented by the GNSS was promoted in the paper with the methods of large field angle, environmental smart adaptation, automatic regulation and control of status, and baseline calibration-meteorological fusion correction. The proposed system provides the functions of real-time identification of environmental conditions, self-selection of the measurement period, complementation of multisource data, and smart correction of monitoring data and realizes the real-time smart acquisition of high-confidence monitoring data in a complex environment.

(2) By heightening the observation pier and adopting a 360° cylindrical lifting window, the monitoring range of the single station is greatly increased. The problems of the low accuracy and slow information feedback under special working conditions are effectively solved through installing the TPS monitoring prism and the GNSS aerial coaxially. Besides, the system allows the environmental conditions to be perceived and judged intelligently through the rain and wind speed sensors, thereby minimizing the impact of meteorological conditions on observation accuracy.

(3) The application results of the Pubugou Hydropower Station project show that the APMSE for the dam points meets the accuracy requirements of the second

deformation monitoring, and the AHMSE meets the accuracy requirements of the third deformation monitoring. The monitoring results of the slope are found to be of high accuracy. The tendency of TPS monitoring data is consistent with that of the GNSS monitoring data in the concurrent monitoring of TPS-GNSS, and the maximum relative error of these data is 9.98% compared with the artificial monitoring data, implying that the data acquired by the system is reliable with high accuracy. Additionally, the reliability of the system is good based on the MTBF results, and the smart system is of significant comprehensive benefits.

(4) The system proposed in this paper is the preliminary study of the smart deformation monitoring in dams. The deformation of dams is easy to be affected by the environmental factors and equipment operation status and the abnormal data will inevitably appear in the monitoring sequence, so how to recognize the anomaly observation values intelligently is the next function to be realized.

Data Availability

All data used to support the findings of this study are available from the corresponding author upon request.

Conflicts of Interest

The authors declare that they have no conflicts of interest.

Acknowledgments

The authors would like to acknowledge the National Key R&D Program of China (no. 2018YFC0407103). The financial support is gratefully acknowledged.

References

[1] F. Raspini, S. Bianchini, A. Ciampalini, M. D. Soldato, and N. Casagli, "Continuous, semi-automatic monitoring of ground deformation using Sentinel-1 satellites," *Scientific Reports*, vol. 8, no. 1, pp. 1–11, 2018.

[2] M. Woźniak and W. Odziemczyk, "Investigation of stability of precise geodetic instruments used in deformation monitoring," *Nephron Clinical Practice*, vol. 104, pp. 79–90, 2017.

[3] D.-S. Xu, Y.-M. Zhao, H.-B. Liu, and H.-H. Zhu, "Deformation monitoring of metro tunnel with a new ultrasonic-based system," *Sensors*, vol. 17, no. 8, p. 1758, 2017.

[4] Y. C. Din, B. Dai, and J. H. Wang, "Field observation of a deep excavation adjacent to subway tunnels," *Journal of Beijing University of Technology*, vol. 34, pp. 492–497, 2008.

[5] Y. Luo, J. Chen, W. Xi et al., "Analysis of tunnel displacement accuracy with total station," *Measurement*, vol. 83, pp. 29–37, 2016.

[6] H. Mohamad, K. Soga, P. J. Bennett, R. J. Mair, and C. S. Lim, "Monitoring twin tunnel interaction using distributed optical fiber strain measurements," *Journal of Geotechnical and Geoenvironmental Engineering*, vol. 138, no. 8, pp. 957–967, 2012.

[7] X. Wang, B. Shi, G. Q. Wei, S. E. Chen, H. H. Zhu, and T. Wang, "Monitoring the behavior of segment joints in a shield tunnel using distributed fiber optic sensors," *Structural Control Health Monitoring*, vol. 25, no. 1, Article ID e2056, 2018.

[8] S. Tazio, F. Paolo, C. Alessandro et al., "Survey and monitoring of landslide displacement by means of L-land satellite SAR interferometry," *Landslides*, vol. 2, pp. 193–201, 2005.

[9] J. Rau, K. Chang, and Y. Shao, "Semi-automatic shallow landslide detection by the integration of airborne imagery and laser scanning data," *Natural Hazards*, vol. 8, pp. 69–80, 2011.

[10] R. A. Kromer, A. Abellán, D. J. Hutchinson, M. Lato, and M. Jaboyedoff, "Automated terrestrial laser scanning with near real-time change detection-monitoring of the Séchilienne landslide," *Earth Surface Dynamics*, vol. 8, 2017.

[11] G. Teza, A. Galgaro, N. Zaltron, and R. Genevois, "Terrestrial laser scanner to detect landslide displacement fields: a new approach," *International Journal of Remote Sensing*, vol. 28, no. 16, pp. 3425–3446, 2007.

[12] G. Pugliesi, M. Aloisi, A. Bonaccorso et al., "The early-warning integrated geodetic system to monitor the Sciara del Fuoco (Stromboli) volcanic landslide," in *Proceedings of European Geosciences Union 2004*, vol. 6, Nice, January 2004.

[13] S. Kelly, "Application of IEEE standards and ATML in TPS development for ministry of defence UK," in *Proceedings of Autotestcon. IEEE.*, pp. 350–354, Ministry of Defence, UK, September 2014.

[14] B.-j. Wang, K. Li, B. Shi, and G.-q. Wei, "Test on application of distributed fiber optic sensing technique into soil slope monitoring," *Landslides*, vol. 6, no. 1, pp. 61–68, 2009.

[15] L. James, C. Adam, B. Geoffrey, and W. Cecilia, "Dimons software for automatic data collection and automatic deformation analysis," in *Proceedings of the 10th FIG International Symposium on Deformation Measurements*, pp. 101–109, Orange, CF, USA, March 2001.

[16] W. Rick, B. Geoffery, and C. Adam, "Alert: a fully automated displacement monitoring system," in *Calgary: the CAMI 2003 Conference*, vol. 9, Calgary, Canada, September 2003.

[17] S. Lv, J. C. Guan, and X. C. Liu, "Application of AutoMoS automatic deformation monitoring system in geotechnical engineering monitoring of south anchor foundation pit of Shuang Yong bridge in Liuzhou," *Geotechnical Investigation & Surveying*, vol. S1, pp. 733–738, 2010, (in Chinese).

[18] Y. P. Yang, Y. H. Qu, H. C. Cai, J. Cheng, and C. M. Tang, "A system for automated monitoring of embankment deformation along the Qinghai-tibet railway in permafrost regions," *Sciences in Cold and Arid Regions*, vol. 7, pp. 560–567, 2015.

[19] Z. L. Zhang, W. S. Mei, and G. H. Di, "Researches on geo-robot deformation monitoring system software for landslides of the three Georges," *Hubei Geology & Mineral Resources*, vol. 16, pp. 56–59, 2002, (in Chinese).

[20] F. Fotovatikhah, M. Herrera, S. Shamshirband, K.-W. Chau, S. Faizollahzadeh Ardabili, and M. J. Piran, "Survey of computational intelligence as basis to big flood management: challenges, research directions and future work," *Engineering Applications of Computational Fluid Mechanics*, vol. 12, no. 1, pp. 411–437, 2018.

[21] C. L. Wu and K. W. Chau, "Prediction of rainfall time series using modular soft computing methods," *Engineering Applications of Artificial Intelligence*, vol. 26, no. 3, pp. 997–1007, 2013.

[22] X.-Y. Chen and K.-W. Chau, "Uncertainty analysis on hybrid double feedforward neural network model for sediment load estimation with LUBE method," *Water Resources Management*, vol. 33, no. 10, pp. 3563–3577, 2019.

[23] X. Li, Y. Li, X. Lu, Y. Wang, H. Zhang, and P. Zhang, "An online anomaly recognition and early warning model for dam safety monitoring data," *Structural Health Monitoring*, vol. 19, no. 3, pp. 796–809, 2020.

[24] R. Taormina and K.-W. Chau, "ANN-based interval forecasting of streamflow discharges using the LUBE method and MOFIPS," *Engineering Applications of Artificial Intelligence*, vol. 45, pp. 429–440, 2015.

[25] S. Shamshirband, S. Hashemi, H. Salimi et al., "Predicting standardized streamflow index for hydrological drought using machine learning models," *Engineering Applications of Computational Fluid Mechanics*, vol. 14, no. 1, pp. 339–350, 2020.

[26] Y. Wang and M. Fang, "Total station trigonometric levelling to replace the three or four levelling of feasibility analysis," *Journal of Wuhan University of Technology*, vol. 38, pp. 1413–1416, 2014.

[27] A. Petry, G. André, and J. Souza, "An approximate nearest neighbors search algorithm for low-dimensional grid locations," *Earth Science Informatics*, vol. 10, pp. 1–14, 2016.

[28] X. Zhi, S. Wang, H. Zhou, S. Zhu, and H. Zhao, "Statistical downscaling of precipitation forecasting using categorized rainfall regression," *Transactions on Atmospheric Science*, vol. 39, pp. 329–338, 2016, (in Chinese).

[29] Ministry of Housing and Urban-Rural Development of China, *GB 50026-2007, Code for Engineering Surveying*, Ministry of Housing and Urban-Rural Development of China, Beijing, China, (in Chinese), 2007.

[30] Ministry of Water Resources of the People's Republic of China, *SL 197-2013, Code for Surveying of Water Resources and Hydropower Engineering*, Ministry of Water Resources of the People's Republic of China, Beijing, China, (in Chinese), 2013.

[31] College of Water Resources & Hydropower, *Comprehensive Analysis of Dam Operation Performance of Pubugou Hydropower Station*, Sichuan University, Chengdu, China, (in Chinese), 2019.

[32] National Development and Reform Commission of China, *Technical Specification for Dam Safety Monitoring Automation*, National Development and Reform Commission of China, Beijing, China, (in Chinese), 2005.